Superhorizon fluctuations and acoustic oscillations in relativistic heavy-ion collisions

Ananta P. Mishra,* Ranjita K. Mohapatra,† P. S. Saumia,‡ and Ajit M. Srivastava§
Institute of Physics, Sachivalaya Marg, Bhubaneswar 751005, India
(Received 9 November 2007; published 5 June 2008)

We focus on the initial-state spatial anisotropies, originating at the thermalization stage, for central collisions in relativistic heavy-ion collisions. We propose that a plot of the root-mean-square values of the flow coefficients $\sqrt{v_n^2} \equiv v_n^{\rm rms}$, calculated in a laboratory fixed coordinate system, for a large range of n from 1 to about 30, can give nontrivial information about the initial stages of the system and its evolution. We also argue that for all wavelengths λ of the anisotropy (at the surface of the plasma region) much larger than the acoustic horizon size $H_s^{\rm fr}$ at the freeze-out stage, the resulting values of $v_n^{\rm rms}$ should be suppressed by a factor of order $2H_s^{\rm fr}/\lambda$. For noncentral collisions, these arguments naturally imply a certain amount of suppression of the elliptic flow. Further, by assuming that initial flow velocities are negligible at thermalization stage, we discuss the possibility that the resulting flow could show imprints of coherent oscillations in the plot of $v_n^{\rm rms}$ for subhorizon modes. For gold-gold collision at 200 GeV/nucleon center-of-mass energy, these features are expected to occur for $n \geqslant 5$, with $n < 4$ modes showing suppression due to being superhorizon. This has strong similarities with the physics of the anisotropies of the cosmic microwave background radiation (CMBR) resulting from inflationary density fluctuations in the universe (despite important differences such as the absence of gravity effects for the heavy-ion case). It seems possible that the statistical fluctuations due to finite multiplicity may not be able to mask such features in the flow data or at least a nontrivial overall shape of the plot of $v_n^{\rm rms}$ may be inferred. In that case, the successes of analysis of CMBR anisotropy power spectrum to get cosmological parameters can be applied for relativistic heavy-ion collisions to learn about various relevant parameters at the early stages of the evolving system.

DOI: 10.1103/PhysRevC.77.064902 PACS number(s): 25.75.−q, 12.38.Mh, 98.80.Cq

I. INTRODUCTION

In the experimental search of the deconfined phase of quantum chromodynamics (QCD), namely the quark-gluon plasma (QGP), one of the most important results has been the observation of the elliptic flow [1,2]. This has given strong evidence of very early thermalization and of the collective behavior of the partonic matter produced in RHICE [3]. (We use RHICE to denote a general class of relativistic heavy-ion collision experiments to distinguish from the Relativistic Heavy-Ion Collider, RHIC, at Brookhaven). Much work has been done to extract physical information about the system from the behavior of the elliptic flow, e.g., equation of state, thermalization time, freeze-out time, etc.

Elliptic flow results from the spatial anisotropy of the thermalized region at the initial stage in a given event with nonzero impact parameter. Anisotropic pressure gradients then lead to anisotropic fluid velocity that results in anisotropic momentum distribution of particle momenta. Elliptic flow measures the second Fourier coefficient of the angular distribution of the particle momenta in the transverse plane. It has also been noticed [4–6] that even in central collisions, due to initial state fluctuations, one can get nonzero anisotropies in particle distribution (and hence in final particle momenta) in a given event, though these will be typically much smaller in comparison to the noncentral collisions. These will average out to zero when a large number of central events are considered. Fluctuations in the elliptic flow resulting from these initial state fluctuations, as well as the resulting modifications in the eccentricity of the initial region have been investigated in the literature [7,8]. In this article, we present a different approach to analyze the flow anisotropies for central events, resulting from these initial-state fluctuations.

It is sometimes mentioned in popular terms that attempts to learn about early stages of phases of matter in RHICE from the observations of hadrons is in some sense similar to the attempts to understand the early stages of the universe from the observations of the cosmic microwave background radiation (CMBR). The surface of last scattering for CMBR is then similar to the freeze-out surface in RHICE. We will argue below that this correspondence is in fact much deeper. There are strong similarities in the nature of density fluctuations in the two cases (with the obvious difference of the absence of gravity effects for RHICE). Following the successes of the analysis of the CMBR anisotropy power spectrum, we argue below that, for central events in RHICE, a plot of the root-mean-square values of the flow coefficients $\sqrt{v_n^2} \equiv v_n^{\rm rms}$, calculated in a laboratory fixed coordinate system, for a large range of n from 1 to about 30, can give nontrivial information about the initial stages of the system and its evolution. In addition, we recall that one of the most important aspects of the density fluctuations in the universe is the coherence effect that eventually results in the remarkable acoustic peaks in the power spectrum of CMBR anisotropies. The source of this lies in the inflationary origin of the density fluctuations leading to production of superhorizon density fluctuations. Some of these eventually

*apmishra@iopb.res.in
†ranjita@iopb.res.in
‡saumia@iopb.res.in
§ajit@iopb.res.in

re-enter the horizon around the decoupling stage and leave these imprints on CMBR anisotropies [9]. We will argue below that, quite similarly, superhorizon fluctuations are present in RHICE as well. However, here they will result in nonzero flow coefficients as spatial anisotropies lead to anisotropic pressure gradients. The anisotropies in the momentum distributions of the particles, especially at large orders of the Fourier coefficients, will capture information about the nature of initial spatial anisotropies, their evolution, and freeze-out.

The article is organized as follows. In Sec. II we discuss the nature of the anisotropies present initially at the stage of equilibration. Section III discusses the basic physics of our model exploring the correspondence with CMBR physics. Section IV incorporates the presence of a finite acoustic horizon in RHICE and discusses the expected suppression of the values of $v_n^{\rm rms}$. Section V discusses expected features in the plot of $v_n^{\rm rms}$ based on the physics of our model. Section VI presents numerical results and conclusions are given in Sec. VII.

II. INITIAL FLUCTUATIONS IN CENTRAL COLLISIONS

As mentioned in the Introduction, the main focus of our analysis is on central events; the considerations can be trivially extended to the noncentral case. Just as for the elliptic flow, here also we consider only transverse fluctuations by assuming Bjorken scaling for the longitudinal expansion. This is a reasonable approximation if the freeze-out, when momentum anisotropies of the particles are frozen out, does not happen too late. For a given central event, azimuthal distribution of particles and energy density are in general anisotropic due to fluctuations of nucleon coordinates as well as due to localized nature of parton production during initial nucleon collisions. As an example, for Au-Au collision at 200 GeV/nucleon center-of-mass energy, we show the contour plot of initial transverse energy density in Fig. 1. This is obtained using HIJING [10]. For parton positions we use random locations inside the volume of the parent nucleon. For partons that are produced by the string systems we position them randomly

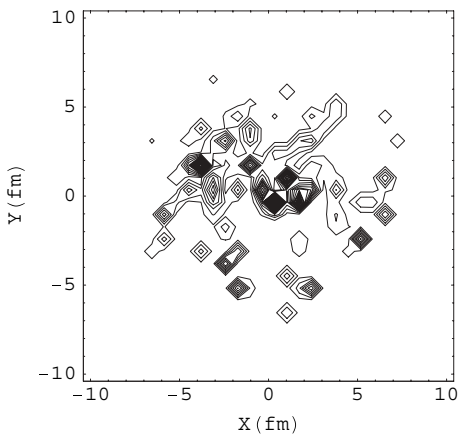

FIG. 1. Contour plot of the initial transverse energy density distribution from HIJING for a given Au-Au collision central event at 200 GeV/nucleon center-of-mass energy.

along the line joining the two nucleons corresponding to the relevant string. The transverse energy density at a given transverse position $\vec{x}$, at proper time $\tau = \tau_{\rm eq}$, is taken as [4],

$$\epsilon_{\rm tr}(\vec{x}, \tau_{\rm eq}) = \frac{1}{\Delta A} \sum_i E^i_{\rm tr} F(\tau_{\rm eq}, p_{\rm tr}) \delta^2(\vec{x} - \vec{x}^i_0 - \vec{v}^i \tau_{\rm eq}) \Delta(y^i), \tag{1}$$

where $\vec{x}^i_0$ denotes the initial transverse coordinates of the ith parton (determined using the coordinates of the parent nucleon in HIJING as discussed above), $E^i_{\rm tr}$ is its transverse energy, $p_{\rm tr}$ the transverse momentum, and $\vec{v}^i$ is its transverse velocity. For the rapidity window we take $\Delta(y^i) = 1$ centered at $y = 0$ [4]. The sum over i includes all partons in a small transverse area element $\Delta A (\simeq 0.5\ {\rm fm}^2)$ at position $\vec{x}$. Following Refs. [4,11] we have included a factor $F(\tau_{\rm eq}, p_{\rm tr}) \equiv 1/(1 + 1/(p_{\rm tr}\tau_{\rm eq})^2)$ to account for the probability of formation of partons with zero rapidity. Figure 1 shows the contour plot of the energy density at $\tau_{\rm eq} = 1$ fm. We assume that by this time the produced partons thermalize and hydrodynamic description becomes applicable for subsequent times (with the energy density decreasing, for $\tau > \tau_{\rm eq}$, due to longitudinal as well as transverse hydrodynamical expansions). We will present results with the transverse energy given as above in Eq. (1). We have also checked the effects of the presence of a smooth background, such as the one representing soft beam-jet component in Ref. [4]. As in Ref. [4], we model it as $\epsilon_{\rm soft} \sim \rho_c[1 - (r_{\rm tr}/R)^2]^{1/2}$, where $r_{\rm tr}$ is the transverse radial coordinate and R is taken as the nucleus size. The central density for this soft component, ρ_c, at $\tau_{\rm eq}$, is varied from 0 up to about 3 GeV/fm^2 [4]. As expected, the presence of this soft component reduces the overall magnitude of the fluctuations and hence the initial anisotropies. However, the qualitative nature of our results do not change with this, as we will discuss later in Sec. IV.

Azimuthal anisotropy of produced partons is manifest in Fig. 1. It is thus reasonable to expect that the equilibrated matter resulting from this parton distribution will also have azimuthal anisotropies (as well as radial fluctuations) of similar level. The process of equilibration will lead to some level of smoothing. However, flow measurements have given very interesting result that thermalization is expected to happen quickly, within a proper time $\tau_{\rm eq} \leqslant 1$ fm for RHIC energies. Hence, no homogenization can be expected to occur beyond length scales larger than this, leading to presence of nonuniformities at the initial stage.

III. BASIC PHYSICS OF THE MODEL

From the discussion in the last section we conclude that inhomogeneities, especially anisotropies with wavelengths larger than the thermalization scale, should be necessarily present at the thermalization stage when the hydrodynamic description is expected to become applicable. This brings us to the most important correspondence between the universe and the RHICE. It is the presence of fluctuations with superhorizon wavelengths. In the universe, density fluctuations with wavelengths of superhorizon scale have their origin in the

inflationary period. Quantum fluctuations of subhorizon scale are stretched out to superhorizon scales during the inflationary period. During subsequent evolution, after the end of the inflation, fluctuations of sequentially increasing wavelengths keep entering the horizon. The largest ones to enter the horizon, and grow, at the stage of decoupling of matter and radiation lead to the first peak in CMBR anisotropy power spectrum.

Figure 1 shows that superhorizon fluctuations should be present in RHICE at the initial equilibration stage itself. The reason these are superhorizon is that the causal horizon is given by $c\tau$. More appropriately, one should be using the sound horizon, $H_s \sim c_s\tau$, where c_s is the sound speed, as we are interested in the flow arising from pressure gradients. At the stage of equilibration, $c\tau_{eq}$ is at most 1 fm, with corresponding acoustic horizon H_s^{eq} being even smaller. Thus every fluctuation of wavelength larger than H_s^{eq} is superhorizon. With the nucleon size being about 1.6 fm, the equilibrated matter will necessarily have density inhomogeneities with superhorizon wavelengths. As the system evolves beyond τ_{eq}, fluctuations of larger wavelengths enter the horizon. We will argue in Sec. IV that the (rms values of) the flow coefficients corresponding to fluctuations that remain superhorizon at the freeze-out stage will be suppressed.

It is important to note that density fluctuations will also be present in the longitudinal direction. However, for partons being created near $z = 0$ (z being the longitudinal coordinate), and subsequently expanding out, one cannot argue that these longitudinal fluctuations are out of causal contact (except possibly in the color glass condensate models [12], as we discuss later). In contrast, the transverse fluctuations are superhorizon because of simultaneous collisions of different (transverse) parts of a system with large transverse dimensions compared to the causal horizon at the thermalization stage (the system being longitudinally Lorentz contracted nuclei, or at the smallest level, colliding nucleons or clusters of nucleons). In this way, the fluctuations leading to the elliptic flow are necessarily superhorizon. As we will see later, they remain superhorizon even at the freeze-out stage, and hence the resulting elliptic flow is necessarily suppressed compared to maximum possible value. This difference between the longitudinal and transverse fluctuations may be important in the context of our model (apart from other differences due to different expansion dynamics in the two directions), as we will discuss later.

To estimate spatial anisotropies for the system as in Fig. 1 we will use the following procedure. As mentioned, we assume that the hydrodynamic description becomes applicable by $\tau = \tau_{eq}$, which we take to be 1 fm. We calculate the anisotropies in the fluctuations in the spatial extent $R(\phi)$ at this stage, where $R(\phi)$ represents the energy-density-weighted average of the transverse radial coordinate in the angular bin at azimuthal coordinate ϕ. We divide the region into 50–100 bins of azimuthal angle ϕ and calculate the Fourier coefficients of the anisotropies in $\delta R/R \equiv (R(\phi) - \bar{R})/\bar{R}$, where $\bar{R}$ is the angular average of $R(\phi)$. Note that in this way we are representing all fluctuations essentially in terms of fluctuations in the boundary of the initial region. Clearly there are density fluctuations in the interior region as well. However, in view of thermalization processes operative within the plasma region, as far as the development of flow anisotropies is concerned, presumably the representation by fluctuating boundary will capture the essential physics. A more careful analysis should include the details of fluctuations in the interior regions and their effects on the evolution of the flow. We will use F_n to denote Fourier coefficients for these spatial anisotropies and use the conventional notation v_n to denote the nth Fourier coefficient of the resulting momentum anisotropy in $\delta p/p$. Here δp represents fluctuation in the momentum p of the final particles from the average momentum, in a given azimuthal angle bin.

An important difference between the conventional discussions of the elliptic flow and our analysis is that here one does not try to determine any special reaction plane on event-by-event basis. A fixed coordinate system is used for calculating azimuthal anisotropies. This is why, as we will see later, averages of F_ns (and hence of v_ns) will vanish when a large number of events are included in the analysis. However, the root-mean-square values of F_ns, and hence of v_ns, will be nonzero in general and will contain nontrivial information. In fact, it is the same as the standard deviation for the distribution of F_ns because the average value of F_ns is zero. This is what is exactly done for the CMBR case also [9]. This is why even when temperature fluctuations are very tiny for CMBR (1 part in 10^5), one is still able to resolve the acoustic peaks. Note that we use v_2 with the present definitions to denote the elliptic flow even though we do not adopt the conventional usage of the eccentricity for defining the corresponding spatial anisotropy. Clearly the procedure described above gives a crude estimate of the spatial anisotropy of the initial plasma region. We have taken other different measures of the spatial anisotropy and, as we will discuss later, it does not affect our results much.

A. Correspondence with CMBR physics: Coherence of fluctuations

Before we proceed any further in analyzing the nature of density fluctuations in RHICE and its similarities with CMBR anisotropies, let us be clear about the relevant experimentally measurable quantities. For the case of the universe, density fluctuations at the surface of last scattering are accessible through their imprints on the CMBR. Thus only for the fluctuations present at the decoupling stage, starting from the short wavelength fluctuations that would have undergone several oscillations until decoupling, including the large wavelength fluctuations that just enter the horizon at decoupling and start growing due to gravity, up to the superhorizon fluctuations, CMBR anisotropies capture imprints of all of them and are observed today [9]. For the RHICE case, the experimentally accessible data is particle momenta that are finally detected. Initial-stage spatial anisotropies are accessible only as long as they leave any imprints on the momentum distributions (as for the elliptic flow) that survive until the freeze-out stage. What one is looking for, therefore, is the evolution of spatial anisotropies of different wavelengths, and corresponding buildup of momentum anisotropies (i.e., essentially different flow coefficients), existing at the freeze-out stage.

The two most crucial aspects of the inflationary density fluctuations leading to the remarkable signatures of acoustic peaks in CMBR are coherence and acoustic oscillations. Let us consider them in turn to see if any such features are expected for RHICE. Let us recall that coherence of inflationary density fluctuations essentially results from the fact that the fluctuations initially are stretched to superhorizon sizes and are subsequently frozen out dynamically. Thus, at the stage of re-entering the horizon, when these fluctuations start growing due to gravity, and subsequently start oscillating due to radiation pressure, the fluctuations start with zero velocity. For an oscillating fluctuation, this will mean that only $\cos\omega t$ term survives. As all the fluctuations, entering the horizon at a given stage, have the same wavelength (by definition), they all are phase locked, coming to zero amplitude simultaneously. In summary, the crucial requirement for coherence of fluctuations is that they are essentially frozen out until they re-enter the horizon [9].

This should be reasonably true for RHICE, especially as we are considering transverse fluctuations. Transverse velocity to begin with is expected to be zero. Though note that with initial-state fluctuations due to fluctuations in nucleon (hence partons) positions and momenta, there may be some residual transverse velocities even at the earliest stages [4]. However, due to averaging, for wavelengths significantly larger than the nucleon size, it is unlikely that the fluid will develop any significant velocity at the thermalization stage. For much larger wavelengths, those that enter (sound) horizon at proper times much larger than $\tau_{\rm eq}$, buildup of the radial expansion will not be negligible. However, our interest is in the presence of any oscillatory modes. For such oscillatory time dependence even for such large wavelength modes, there is no reason to expect the presence of $\sin\omega t$ term at the stage when the fluctuation is just entering the sound horizon.

B. Acoustic oscillations

Let us now address the possibility of the oscillatory behavior for the fluctuations. In the universe, attractive forces of gravity and counter balancing forces from radiation pressure (with the coupling of baryons to the radiation) lead to acoustic oscillations [9]. For RHICE, there is no gravity, but there is a nonzero pressure present in the system. First let us just follow the conventional analysis as in the case of elliptic flow. We know that, as the spatial anisotropy decreases in time by the buildup of momentum anisotropy (starting from isotropic momentum distribution), it eventually crosses zero and becomes negative. This forces momentum anisotropy to saturate first (when spatial anisotropy becomes zero) and then start to decrease. In principle, one could imagine momentum anisotropy to decrease to zero, becoming negative eventually. The whole cycle could then be repeated, resulting in an oscillatory behavior for the spatial anisotropy as well as for the momentum anisotropy, possibly with decreasing amplitude.

Unfortunately, the situation is not that favorable. For the elliptic flow, in hydrodynamic simulations one does see saturation of the flow and possibly turn over [13], but the momentum anisotropy does not become zero, and there is never any indication of an oscillatory behavior. The important thing to note here is that this primarily happens because of the buildup of the strong radial flow by the time elliptic flow saturates and subsequently freezes out. This can be seen from the evolution of transverse velocity in hydrodynamics simulations [13]. One then would like to know whether the same fate is necessarily true for fluctuations of much smaller wavelength as well. At this stage it is important to be clear about the relevant freeze-out time $\tau_{\rm fr}$ for the flow. If radial expansion becomes very strong then pressure gradients, or any interface tension effects (as we will discuss below), may not be able to significantly affect fluid flow anisotropies. Flow anisotropy would then essentially freeze out even if chemical or thermal freeze-out may not have occurred yet. For elliptic flow this is usually accounted for by referring to the flow buildup time scale of order R/c_s, where R represents the initial average transverse extent of the region [1]. This is the time scale when transverse expansion is expected to become strong. For central collisions, we will take $R = \bar{R}(\tau_{\rm eq}) \equiv \bar{R}$, which was earlier defined as the energy-density-weighted average of the transverse radial coordinate at $\tau = \tau_{\rm eq}$. For Au-Au collision at 200 GeV, the value of $\bar{R}$ is obtained to be about 3 fm from HIJING. This gives us $\tau_{\rm fr} = \bar{R}/c_s + \tau_{\rm eq} \simeq 6$ fm. (We use velocity of sound $c_s = 1/\sqrt{3}$. Later we will discuss the effects of changing the value of c_s.) Note that this value of $\tau_{\rm fr}$ is much smaller than the value of the thermal freeze-out time at these energies that is expected to be of order 12 fm. Certainly flow anisotropies have to freeze by the stage of thermal freeze-out. We have also used the value of $\tau_{\rm fr}$ to be 12 fm and it does not change our results, as we will discuss later. We will use the freeze-out stage as given by $\tau_{\rm fr} - \tau_{\rm eq} = \bar{R}/c_s$. The size of the acoustic horizon at $\tau = \tau_{\rm fr}$ is then simply $H_s^{\rm fr} = c_s(\tau_{\rm fr} - \tau_{\rm eq}) = \bar{R} \simeq 3$ fm for Au-Au collision at 200 GeV. We take the sound horizon to be proportional to the proper time elapsed since the stage of equilibration given by $\tau_{\rm eq}$, because this is the stage when hydrodynamics becomes applicable. Before $\tau_{\rm eq}$, individual particles can interact with each other, so in principle one could define a nonzero causal horizon size for individual particles. However, there is no sense in which one can talk about the interaction of different collective modes before $\tau_{\rm eq}$. Hence it seems reasonable that the acoustic horizon, as appropriate for these collective modes, is defined in terms of time elapsed from $\tau_{\rm eq}$. In the present case with $\tau_{\rm eq}$ being very small, of order 1 fm, our results remain almost unchanged even if we take $H_s^{\rm fr} = c_s\tau_{\rm fr}$. Important point to note is that this time $\tau_{\rm fr}$ remains fixed for a given collision, irrespective of the wavelength λ of the fluctuation considered. For small wavelengths, if the time scale for the buildup of momentum anisotropy is much smaller than $\tau_{\rm fr}$, then oscillations may be possible before the flow freezes out at $\tau_{\rm fr}$. Consider spatial anisotropy with a wavelength that is much shorter than $H_s^{\rm fr}$ at the freeze-out stage, say λ being of order 2 fm; see Fig. 2. One will expect that due to unequal initial pressure gradients in the two directions ϕ_1 and ϕ_2, momentum anisotropy would have built up in these two directions in a relatively short time. Most importantly, we expect that spatial anisotropy should reverse sign in time of order $\tau_{\rm flip} \simeq \lambda/(2c_s) \simeq 2$ fm. The momentum anisotropy should then reach saturation before this time and start to

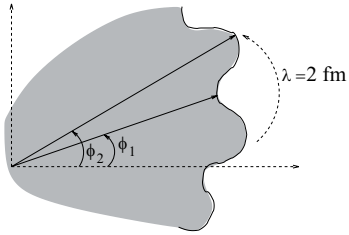

FIG. 2. Schematic diagram of a part of the region showing spatial anisotropies of small wavelength.

decrease by $\tau \simeq \tau_{\rm flip}$. Due to short time scale of evolution here, radial expansion may still not be most dominant and there may be possibility of momentum anisotropy changing sign, leading to some sort of oscillatory behavior.

The arguments presented above are very qualitative, but they allow a possibility of oscillatory behavior for the spatial anisotropy (i.e., fluctuations) of short wavelengths and hence possibly for the flow anisotropy. An entirely different line of argument supporting oscillatory behavior can be given as follows. As the QGP region is surrounded by the confining vacuum (or the hadronic phase), one may expect some sort of interface, with nonzero surface tension, to be present at the boundary of the QGP region [14]. This is necessarily true if the confinement-deconfinement transition is of first order. Once we assume an interface present at the boundary of the QGP region, its surface tension will induce oscillatory evolution given initial fluctuations present (as shown in Figs. 1 and 2). For a relativistic domain wall such fluctuations propagate with speed of light. However, here one will be dealing with an interface bounding a dense plasma of quarks and gluons. In such a case it will be reasonable to expect that tiny perturbations on the interface will evolve with speed of sound (appropriate for the QGP region enclosed). The interface will eventually disappear after the quark-hadron phase transition stage. We mention here that the contributions of any such interface could also be present (though, possibly small, relatively) for the conventional calculations of the elliptic flow for noncentral collisions. Also, effects of surface tension will be more prominent for lower energy collisions, and the considerations of our model can be applied for such low-energy heavy-ion collision experiments.

IV. ACOUSTIC HORIZON AND DEVELOPMENT OF FLOW

One important aspect of these fluctuations is that of *horizon entering*. In the case of the universe every fluctuation leads to CMBR anisotropies even when it is superhorizon. This is because these are density fluctuations and local thermal equilibrium directly leads to associated CMBR temperature fluctuations. The importance of horizon entering there is for the growth of fluctuations due to gravity. This leads to an increase in the amplitude of density fluctuations, with subsequent oscillatory evolution, leaving the imprints of these important features in terms of acoustic peaks [9]. For RHICE, there is a similar (though not the same, due to absence of gravity here) importance of horizon entering. Azimuthal spatial anisotropies are not directly detected. They are detected only when they are transferred to the momentum anisotropies of particles. Consider first an anisotropy of wavelength λ much larger than the acoustic horizon at freeze-out $H_s^{\rm fr}$. The evolution of fluid velocity (particle momenta) depends on pressure gradients. However, pressure gradients at $\tau = \tau_{\rm fr}$ should be calculated only within regions of size $H_s^{\rm fr}$ as outside regions could not have affected the region under consideration. Consider, for simplicity, fluid expanding radially with initial transverse velocity v being zero. Then keeping only terms that are of first order in v (and neglecting $\partial P/\partial\tau$ term) the Euler's equation gives [15]

$$\frac{\partial v}{\partial \tau} = \frac{-1}{(\rho + P)} \frac{\partial P}{\partial r}, \tag{2}$$

where ρ is the energy density, P is the pressure, and r is the transverse radial coordinate. This equation illustrates the expected buildup of the flow velocity being proportional to the pressure gradient. However, for a spatial anisotropy with $\lambda \gg H_s^{\rm fr}$ the angular variation of the pressure gradient should be calculated using only information within a region of size $H_s^{\rm fr}$. We will argue below that we can approximate the angular variation of the relevant pressure gradient, operative within length scale of $H_s^{\rm fr}$, to be a fraction of order $H_s^{\rm fr}/(\lambda/2)$ of its value arising from the full magnitude of the spatial anisotropy.

Presence of such a suppression factor is most naturally seen for the case when the build up of the anisotropies in the flow from spatial anisotropies is dominated by the surface tension of the interface bounding the QGP region. For an anisotropy of wavelength λ, the maximum and minimum of spatial extent are separated by distance $\lambda/2$ at the surface (see, Fig. 2). After half oscillation we expect the reversal of the anisotropy, i.e., maximum will become minimum and minimum will become maximum. However, if the acoustic horizon $H_s^{\rm fr} = c_s(\tau_{\rm fr} - \tau_{\rm eq}) \ll \lambda/2$, then this full reversal is not possible. Starting from the position of the initial maximum amplitude, the relevant amplitude for oscillation is only a factor of order $H_s/(\lambda/2)$ of the full amplitude. Thus, we conclude that the resulting anisotropy of the flow for this particular mode will be suppressed by a factor f of order $2H_s^{\rm fr}/\lambda$.

Let us now consider the situation when flow anisotropies result from the pressure gradients, as in the conventional calculations of the elliptic flow for noncentral events. There, the difference in the pressure gradients in the two directions (x and y) arises from the difference in the values of the semiminor axis a and semimajor axis b of the elliptical transverse overlap region. A given central pressure P_c then gives different pressure gradients in the x and y directions. However, it should be obvious that for times at which the acoustic horizon is much smaller than a, or b, the value of P_c should be irrelevant. There is no way that the surface of QGP would get any information about P_c for $H_s = c_s\tau \ll a, b$. Only relevant pressure gradients should be calculated using interior pressure value at distances of order $c_s\tau$ starting from the surface in the x and the y directions. For example, for our case of central events, let us parametrize the radial profile of the pressure, along a particular direction ϕ, as

$$P(r) = P_c \exp\left(\frac{-r^2}{2\sigma_\phi^2}\right) \tag{3}$$

with σ_ϕ varying with azimuthal angle giving the spatial anisotropy. For calculating the pressure gradient at small time τ (measured from τ_{eq}), at $r = R_0$ at the surface region, we can use the following estimate.

$$\frac{\partial P}{\partial r} \simeq \frac{P(R_0 - c_s\tau) - P(R_0)}{(-c_s\tau)} \simeq -P_c \exp\left(\frac{-R_0^2}{2\sigma_\phi^2}\right)\left[\frac{R_0}{\sigma_\phi^2} + \frac{c_s\tau}{2\sigma_\phi^2}\left(\frac{R_0^2}{\sigma_\phi^2} - 1\right)\right]. \quad (4)$$

This example shows that $-\partial P/\partial r$, at the surface for $R_0 > \sigma_\phi$, starts from a small value at $\tau = 0$ (again τ measured from $\tau_{\rm eq}$) and increases with the sound horizon as $c_s\tau$, although the growth of velocity also requires the value of $\rho + P$ (whose average value also increases with τ), which in some sense provides the inertia of the fluid element. However, we can focus on a particular fluid element near the surface and estimate its acceleration using above pressure gradient. Thus, though we are calculating the average pressure gradient using an increasing region with τ (as $c_s\tau$), we do not consider the average velocity of this entire region. We are always focusing on the region near $r \simeq R_0$ near the surface. The fact that the magnitude of the average pressure gradient increases in time suggests that the pressure gradient operative at $r \simeq R_0$ should also increase in time. Note that Eq. (3) is only meant to give the initial profile of the pressure and it would be incorrect to use it to calculate $\partial P/\partial r$ (say, at R_0) at a later stage, by which the interior higher pressure will be expected to affect the fluid flow at the surface. [For $\tau = 0$, Eq. (4) gives the same result for $\partial P/\partial r$ as directly obtained from Eq. (3).] Also note that the particular dependence on τ in Eq. (4) is due to our specific choice of pressure profile in Eq. (3). For example, a linear r dependence for the pressure in Eq. (3) would give constant pressure gradient in time for Eq. (4) by the above estimate. However, the pressure profile of the sort in Eq. (3) is more representative of the expected profile than a linear dependence. (Though, even here, for interior regions with $R_0 < \sigma_\phi$, one will conclude that $-\partial P/\partial r$ decreases in time.) We mention that the physical considerations discussed above may be relevant for the early rise of the pressure gradients seen in the simulations in Ref. [16].

The length scale relevant for considering the azimuthal variation of the flow is the wavelength λ of the fluctuation under consideration. Again, for a spatial anisotropy of wavelength λ near the surface of the QGP region, we would like to know flow buildup at two regions separated by $\lambda/2$. These two regions will have access to a common value of central pressure after a time $\tau_{\rm cmn}$ with $\tau_{\rm cmn} - \tau_{\rm eq} \simeq \lambda/(2c_s)$. This implies that as far as azimuthal anisotropy of the pressure gradient, and the resulting flow, are concerned, there should be no suppression in the anisotropy after time $\tau_{\rm cmn}$ arising from the considerations of horizon entering. In some sense, this fluctuation would be said to have "entered the horizon" after $\tau_{\rm cmn}$. For $\tau_{\rm cmn} = \tau_{\rm fr}$ this means that the largest wavelength mode that will be unsuppressed will have $\lambda_{\rm max} \simeq 2c_s(\tau_{\rm fr} - \tau_{\rm eq})$.

The above discussion leads us to the conclusion that for superhorizon fluctuations (at freeze-out stage), full momentum anisotropy $(v_n)_{\rm max}$, as expected from hydrodynamics, will not be developed, and only a fraction f of the maximum possible anisotropy will develop. In terms of the corresponding flow coefficients, for modes with $\lambda/2 \geqslant H_s^{\rm fr}$, we expect,

$$(v_n)_{\rm observed} = \frac{2H_s^{\rm fr}}{\lambda}(v_n)_{\rm max}, \quad (5)$$

where $\lambda \sim 2\pi\bar{R}^{\rm fr}/n (n \geqslant 1)$ is the measure of the wavelength of the anisotropy corresponding to the nth Fourier coefficient. Here $\bar{R}^{\rm fr}$ represents the transverse radius at the stage $\tau_{\rm fr}$. Using the rough estimate of the rate of change of the transverse velocity to be about 0.1 fm^{-1} at the early stages at these energies [13], we can estimate $\bar{R}^{\rm fr} \simeq \bar{R} + 0.05(\tau_{\rm fr} - \tau_{\rm eq})^2 = \bar{R}(1 + 0.05\bar{R}/c_s^2)$. Here $\bar{R} \equiv \bar{R}(\tau_{\rm eq}) = c_s(\tau_{\rm fr} - \tau_{\rm eq})$, as discussed above. The largest wavelength $\lambda_{\rm max}$ of spatial anisotropy that will have chance to develop to its maximum hydrodynamic value is, therefore, $\lambda_{\rm max} \simeq 2H_s^{\rm fr} = 2c_s(\tau_{\rm fr} - \tau_{\rm eq}) = 2\bar{R}(\tau_{\rm eq})$. This gives us the corresponding minimum value $n_{\rm min}$ of n below which flow coefficients should show suppression due to being superhorizon,

$$n_{\rm min} = \pi\left[1 + \frac{0.05\bar{R}(\tau_{\rm eq})}{c_s^2}\right]. \quad (6)$$

V. EXPECTED FEATURES IN PLOTS OF $v_n^{\rm rms}$

First we would like to emphasize the important lessons from CMBR analysis that we are proposing to use for RHICE. As we are considering central events, associated anisotropies will be small. Thus we will need large amount of statistics to be able to see any nontrivial features, especially the possibility of oscillations, etc. An important thing to realize is that we cannot take averages of the Fourier coefficients, as these will simply be zero when large number of events are included. Note that our analysis is being done in a laboratory fixed frame. For elliptic flow, one defines an event plane and a special direction given by the impact parameter and then calculates average spatial anisotropy. There is no such direction for a central event. The correct measure of the spatial anisotropy here is to take the root-mean-square values of the Fourier coefficients taken for the whole ensemble of events. As the average value of F_ns is zero, it is the same as the standard deviation for the distribution of F_ns. This is what is exactly done for the CMBR case [9]. This is why even when temperature fluctuations are very tiny for CMBR (1 part in 10^5), one is still able to resolve the acoustic peaks. One important difference that is in the favor of RHICE is the fact that for the CMBR case, for each l mode of the spherical harmonic, there are only $2l + 1$ independent measurements available, as there is only one CMBR sky to observe. In particular for small l values this leads to the accuracy limited by the so-called cosmic variance [9]. In contrast, for RHICE, each nucleus-nucleus collision (with same parameters like collision energy, centrality etc.) provides a new sample event (in some sense like another universe). The accuracy, for any Fourier mode, is only limited here by the number of events one includes in the analysis. Therefore it should be possible to resolve any signal present in these events as discussed in this article. Note, due to the absence of any special reflection symmetry here (which was present in the elliptic flow case) there is no reason to expect that only

even flow coefficients will be present. In our case all flow coefficients give nonzero contributions to $v_n^{\rm rms}$, and the sin terms give same values as the cos terms. In the plots of $v_n^{\rm rms}$ in the next section, we show the sum of these two contributions, i.e., square root of the sum of the squares of the sin term and the cos term.

We have argued in the last section that for fluctuations with $n < n_{\rm min}$ [Eq. (6)] we expect suppression of values of $v_n^{\rm rms}$. For the Au-Au collision at 200 GeV, with $\bar{R}(\tau_{\rm eq}) \simeq 3$ fm, we get $n_{\rm min} \simeq 4.5 \simeq 5$. Note in particular that this implies that the mode with $n = 2$, which corresponds to the elliptic flow, will be expected to be suppressed by a factor of order $f \simeq 1/2$. This suppression is roughly of same order as the suppression factor for the elliptic flow discussed in the literature [8,17]. Note, however, that in Refs. [8,17], the suppression of the elliptic flow is related to the nonzero value of the Knudsen number arising from incomplete thermalization. One will then expect that the final suppression should be a combination of both of these factors. Note also that if velocity of sound c_s decreases, taking flow freeze-out to occur at fixed time, the acoustic horizon H_s will be smaller. The suppression factor in Eq. (5) will be stronger, leading to a smaller flow. We can also see from Eq. (6) that decreasing c_s increases $n_{\rm min}$, leading to larger suppression for the elliptic flow (by a factor $\simeq 2/n_{\rm min}$). This is consistent with the findings in Ref. [8]. We mention here that the scaling of v_2 with $c_s(t - t_0)$ is known in literature; see Ref. [8]. What we have discussed above essentially says that similar scaling, when applied to spatial anisotropies with different wavelengths (i.e., different Fourier modes), will lead to a multiplicative factor given by Eq. (5) for the corresponding flow anisotropies.

For all wavelengths smaller than $\lambda_{\rm max}$, spatial anisotropy should be able to develop into its full hydrodynamic value (apart from the effects such as incomplete thermalization [8,17], as mentioned above). For the case of elliptic flow several studies have shown that for near central events, the momentum anisotropy is related to the initial spatial anisotropy by a proportionality constant of about 0.2 [18]. The relation between the Fourier coefficients of the spatial anisotropy and resulting momentum anisotropy in our model can be obtained only using a full hydrodynamical simulation, with proper accounts of any surface tension, as well as factors such as horizon crossing, etc., to properly account for the physics discussed here. In the absence of such a simulation, we make a strong assumption here that all Fourier coefficients for momentum anisotropy are related to the corresponding coefficients for spatial anisotropy by roughly the same proportionality factor, which we take to be 0.2 for definiteness. As we will see, this choice gives us reasonably good agreement with the results for v_2 in the literature for (almost) central events. Further, for simplicity we evaluate the Fourier coefficients for the spatial anisotropy, F_ns, at the initial stage $\tau = \tau_{\rm eq}$. In principle one can consider relating the final flow coefficients v_n (which freeze-out at $\tau = \tau_{\rm fr}$) to the F_ns at later stages. For example, we could estimate F_ns at $\tau = \tau_{\rm fr}$, or more appropriately, for each mode n we could evaluate F_n at the stage of its horizon entering (meaning the stage when the sound horizon equals $\lambda/2$ for that mode). Such estimates will require suitable modeling of transverse expansion and we hope to do that in a future work. For now we wish to emphasize that the ambiguity in relating v_n to F_n does not affect the important qualitative aspects of our results, as we will discuss later.

As the fluctuation with $\lambda = \lambda_{\rm max}$ will be expected to achieve its maximum value at the freeze-out, we expect that for all wavelengths $\lambda < \lambda_{\rm max}$, if any oscillatory behavior is present, as discussed above, then it will lead to an additional factor of $\cos\omega\tau$ (with τ measured from $\tau_{\rm eq}$) in the Fourier coefficient, where $\omega = 2\pi c_s/\lambda$ is the frequency of oscillation for the relevant fluctuation. This will imply that the fluctuations which will have their maximum values at the freeze-out stage will have wavelengths given by $\lambda_N \sim \lambda_{\rm max}/N$, where $N = 1, 2, 3\cdots$ is a positive integer. Note, this assumes that oscillation time scale for these fluctuations is governed by the sound speed that will be expected if oscillations are dominated by the interface tension at the QGP boundary. For the oscillations resulting from the reversal of flow due to anisotropic pressure gradients (as discussed above), the oscillation time scale may be different.

VI. NUMERICAL RESULTS

We are now ready to discuss our results. We have generated events using HIJING and we present sample results for Au-Au collision at 200 GeV/nucleon center-of-mass energy. Figure 3 shows plots where averages are taken over 10,000 events. The solid curve in Fig. 3 shows the root-mean-square values $v_n^{\rm rms}$ of the flow Fourier coefficients that are obtained from spatial F_ns using proportionality factor of 0.2 (as discussed above). F_ns are calculated directly from events as depicted in Fig. 1 with the rapidity constraints as discussed for Eq. (1). For comparison, we show here the plot of $v_n^{\rm rms}$ obtained from F_ns when partons are distributed in a nucleus size region with uniform probability (dotted plot in Fig. 3). The p_T distribution of partons for this dotted plot in Fig. 3 is taken to be the same as that obtained from

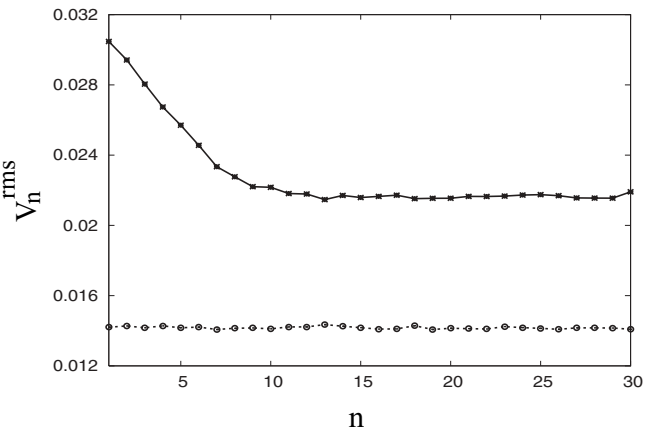

FIG. 3. These plots represent $v_n^{\rm rms}$ calculated from the Fourier coefficients F_ns of the spatial anisotropy using a proportionality factor of 0.2 as discussed in the text. Plots show smooth joining of the values of $v_n^{\rm rms}$ and obtained using 10,000 events from HIJING. Solid curve is obtained using parton positions from HIJING as discussed for Eq. (1). Dotted curve is obtained with a uniform distribution of parton positions in a nucleus size region.

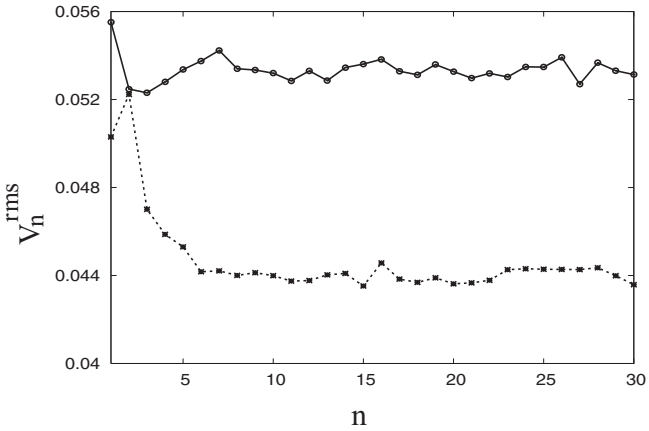

FIG. 4. These plots represent the root-mean-square values of the Fourier coefficients of the momentum anisotropy directly calculated using momenta of final particles from HIJING (with 15,000 events). Dotted plot corresponds to particles with no momentum cuts, whereas the solid plot corresponds to the case when only particles with low p_T ($\leqslant$200 MeV) are included.

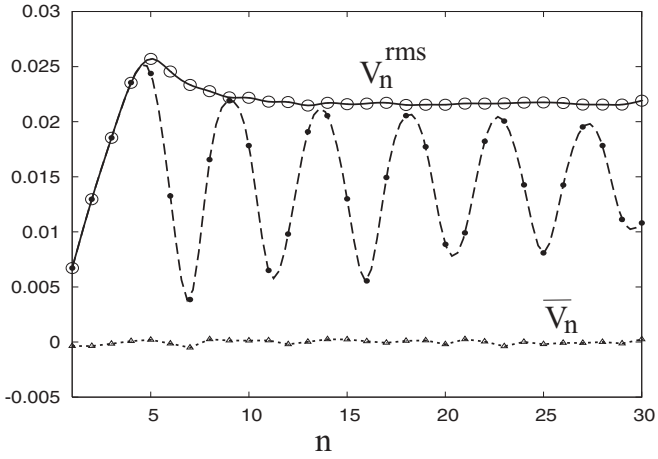

FIG. 5. These plots are obtained from the values of $v_n^{\rm rms}$ of the solid plot in Fig. 3 by including various factors representing the physics of acoustic horizon and coherence, etc., as discussed in the text. Solid curve shows the plot that includes the suppression factor given in Eq. (5), whereas the dashed curve includes an additional $\cos\omega\tau$ factor. Dotted curve represents the average values $\bar{v}_n$ (corresponding to solid plot in Fig. 3). Note that the plots in this figure show only the modeling of the type of suppression factor and oscillations discussed in the text, which are superimposed on the solid plot in Fig. 3.

HIJING. We see that the resulting values of $v_n^{\rm rms}$ are significantly smaller than the values shown by the solid plot in Fig. 3. Also, the plot of $v_n^{\rm rms}$ vs. n is flat as shown by the dotted curve in Fig. 3, in contrast to the nontrivial shape of the solid plot. We have also considered uniform energy distribution among partons, along with uniform probability distribution for their positions. This leads to even smaller values for $v_n^{\rm rms}$ compared to the dotted curve in Fig. 3 (about 15% smaller), and the plot remains flat. This suggests that statistical fluctuations in parton positions may remain subdominant and a genuine fluctuation in parton positions (as depicted in Fig. 1) may be visible by the nontrivial shape of the solid plot in Fig. 3.

We have also calculated the root-mean-square values of the Fourier coefficients of the momentum anisotropy directly using the momenta of final particles from HIJING, using same rapidity window as for plots in Fig. 3. These are shown by the plots in Fig. 4. For the sake of consistency, we denote these also by $v_n^{\rm rms}$. Here averages are taken over 15,000 events. The dotted plot represents contributions from all final particles. Note that this curve is not entirely flat as should be expected from an isotropic momentum distribution with white noise. Though fractional change for low values of n is small compared to the solid plot in Fig. 3. The plot becomes almost flat when only low p_T ($\leqslant$200 MeV) particles are included, as shown by the solid plot, suggesting that larger values of $v_n^{\rm rms}$ at lower n in the dotted plot are due to jet correlations. Overall larger values of $v_n^{\rm rms}$ for the solid plot compared to the dotted plot here are due to smaller number of particles in each event with low p_T selection leading to larger fluctuations.

In Fig. 5 we replot the values of $v_n^{\rm rms}$ (corresponding to the solid plot in Fig. 3) with the inclusion of various physical factors such as finite acoustic horizon and coherence of fluctuations as discussed in previous sections. The solid curve shows plot of values of $v_n^{\rm rms}$ (as given by the solid curve in Fig. 3) with the inclusion of suppression factor [Eq. (5)] for superhorizon fluctuations, and the dashed curve includes this suppression factor as well as the $\cos\omega\tau$ oscillatory factor for subhorizon anisotropies. The dotted curve, which is close to zero, shows the plot of average values of v_n (instead of root-mean-square value) corresponding to the solid plot in Fig. 3. Note that various plots here represent smooth joining of the points obtained at integer n. This is why the dashed plot in Fig. 5 that includes $\cos\omega\tau$ factor does not reach zero [which, from Eq. (6) will typically occur at fractional values of n].

The plots in Figs. 3–5 have several important features. First note, in Fig. 3, a systematic decrease in the values of $v_n^{\rm rms}$ as n increases, starting from a significantly nonzero value. The errors in the values of $v_n^{\rm rms}$ are very small (e.g., less than about 2% for the solid plot in Fig. 3). The overall shape of this plot may contain nontrivial information about the early stages of the system and its evolution. For example, the flattening of the curve by $n \simeq 10$ may be indicative of a qualitative change in the distribution of the corresponding initial anisotropies with wavelengths smaller than about 2 fm [i.e., with wavelengths, as given after Eq. (5) with $\bar{R}^{\rm fr}$ replaced with $\bar{R}(\tau_{\rm eq}) = 3$ fm as the plots in Fig. 3 are obtained from F_ns at $\tau_{\rm eq}$]. As we discussed above, the flat shape of the dotted curve in Fig. 3 corresponding to uniformly distributed partons, and relatively smaller values of $v_n^{\rm rms}$ for this case, imply that statistical fluctuations due to finite particle numbers may not dominate over the nontrivial shape of the solid plot in Fig. 3. As we discussed above, the nontrivial shape of the dotted plot in Fig. 4 (for direct momentum anisotropy of the final particles from HIJING) is due to high p_T particles. This is evidenced by the flatter shape of the solid curve in Fig. 4 where only low p_T particles are included. The situation for the solid plot in Fig. 3 (and hence for the plots in Fig. 5) is different. Here the nontrivial shape of the plot does not change much even when p_T values of initial

partons is constrained to be low (e.g., $\leqslant$350 MeV, lowering this value further leaves very few partons as initial partons do not have very low p_T for center-of-mass energies used here). Such a nontrivial shape of the solid curve in Fig. 3 should, therefore, directly relate to nontrivial nature of fluctuations present initially.

Another important aspect, which may also be reasonably robust in our model, is the first peak shown by the solid plot in Fig. 5 at $n \sim 5$. As we had seen, the suppression factor in Eq. (5) becomes one for $\lambda \leqslant \lambda_{\max}$, with $\lambda_{\max}$ corresponding to $n \simeq 5$ mode. Note that the exact location of this peak is determined by the value of $n_{\min}$ [Eq. (6)] as well as the shape of the solid curve in Fig. 3. This peak contains information about the freeze-out stage, being directly related to the sound horizon size at that stage. (In this sense, this peak is similar to the first peak observed for CMBR anisotropies, which contains information about the stage of decoupling [9].) The dashed plot denoting oscillatory behavior will be the thing to look for and the plot (which only models the oscillations) shows that with enough statistics, one should be able to observe it if it is present. We emphasize again that our assumption of using the same proportionality constant (0.2) for all v_ns only affects the overall shape of the solid curve in Fig. 3 and consequently the shapes of other two curves in Fig. 5. It has no bearing on the existence of any of the peaks, especially the first peak. Average values $\bar{v}_n$ of v_n, shown by the dotted curve in Fig. 5, are close to zero, as expected. This also shows that we have enough statistics to control fluctuations due to statistical errors. We have not discussed any dissipative effects that are known to affect the transverse expansion, hence the flow, in crucial manner [19]. For example, it is known that viscosity reduces elliptic flow [20]. Presumably such effects could lead to decreasing amplitude of $v_n^{\rm rms}$ for these plots for large n, especially one should expect damped oscillations, hence decreasing heights for the peaks at large n.

For near central collisions (with impact parameter $b \simeq$ 2 fm) the elliptic flow has been estimated earlier in simulations [6]. The standard deviation for values of v_2 is found to be $\sigma \simeq 0.013$ [6]. This is consistent with the experimental results [18]. The plots of $v_n^{\rm rms}$ in Fig. 5 show that the value we obtain for $n = 2$ is in reasonably good agreement with these values quoted in the literature. Note that the agreement is better for curves in Fig. 5 that include the suppression factor as given in Eq. (5), as compared to the solid curve in Fig. 3 that does not include this factor. Note that we do not attempt to compare $\bar{v}_2$ because in Refs. [6,18] $\bar{v}_2$ is obtained in the usual manner by determining the event plane for events with small but nonzero impact parameter. In contrast, in our case the impact parameter is strictly zero and no special directions are determined on event-by-event basis. Presumably the comparison of the standard deviations is not affected much by this difference.

We have repeated these calculations by taking other measure of spatial anisotropies, for example, given by a uniform fluid density approximation and taking spatial extent in a given ϕ bin to be proportional to the transverse energy in that bin. For this case, the overall numerical values increase by about 20%, whereas the overall shapes of the curves remain essentially similar. Therefore, the qualitative aspects of our results seem to be reasonably independent of the specific technique chosen to represent the spatial anisotropies. The effects of adding a smooth background for the transverse energy density [4], as discussed in Sec. II, are as expected: It reduces fluctuations, leading to an overall decrease in the values of $v_n^{\rm rms}$. Decrease is stronger at smaller n. However, the overall shape of the curves remains essentially unchanged. Thus the main features of our results remain unaffected. Also, because we calculate anisotropies in the energy-density-weighted average of radial coordinate, only the ratio of this soft energy density to $\epsilon_{\rm tr}$ [Eq. (1)] is relevant. As the fraction of this soft background is increased, the values of $v_n^{\rm rms}$ further decrease. When the contribution of smooth background is of the same order as that given by Eq. (1) (which happens with $\rho_c \simeq 3$ GeV/fm^2), then values of $v_n^{\rm rms}$ are reduced by about a factor of 4 for small n and by a factor of about 3 for large n.

We have checked the effects of varying various parameters on the shape of these curves. We briefly quote some results here; a more detailed investigation and analysis will be done in a future work. We have considered a larger value of $\tau_{\rm fr}$(= 12 fm) [for a given $\bar{R}(\tau_{\rm eq})$] and our results remain almost unchanged. Much larger values of $\tau_{\rm fr}$(= 20 fm) shifts the first peak to larger n (with corresponding shifts in the other peaks) due to increase in the average transverse velocity, and the peak becomes less prominent primarily due to the flattening of the overall plot of $v_n^{\rm rms}$ for large n. Interestingly, the effects of changing $\tau_{\rm eq}$ are more prominent in our model. With $\tau_{\rm eq} =$ 0.2 fm, we get an increase in the values of $v_n^{\rm rms}$ for small n and a decrease for large n (compared to the case with $\tau_{\rm eq} = 1$ fm). An increase in $v_n^{\rm rms}$ for smaller $\tau_{\rm eq}$ is natural to expect as fluctuations in parton positions are more localized with less free-streaming [Eq. (1)]. The flattening of the overall plot (as in Fig. 3) happens at a larger n for smaller $\tau_{\rm eq}$. This possibly again corresponds to the changeover in the behavior of fluctuations, now happening at much shorter wavelengths (hence large n) due to less free streaming. This may also be responsible for the smaller values of $v_n^{\rm rms}$ for large n, as for such short wavelengths, the fluctuations may be decreased due to the corresponding parton density being larger when free streaming is smaller. Increasing $\tau_{\rm eq}$ to 2.0 fm leads to an overall decrease in the values of $v_n^{\rm rms}$ (decrease is stronger at smaller n, about 20%). Also, the flattening of the curve now happens at smaller n.

The peak position, as governed by $n_{\min}$ given in Eq. (6) (combined with the shape of the decreasing overall curve of $v_n^{\rm rms}$), is sensitive to the value of sound speed c_s. Decreasing c_s shifts the first peak to larger n, with corresponding shifts in the successive peaks. Thus, the location of these peaks can give important information about the equation of state during the early stages. Increasing rapidity window decreases the values of $v_n^{\rm rms}$ for all n, presumably due to larger number of particles leading to less fluctuations. (With $\Delta y = 2$ in our model, values of $v_n^{\rm rms}$ decrease by about 30%.) Increasing center-of-mass energy also leads to an overall decrease in the values of $v_n^{\rm rms}$, again, possibly due to larger number of partons and hence reduced initial anisotropies. It also leads to a slight shift of the peaks to larger n. This happens due to larger value of $\bar{R}$ as can be seen from Eq. (6). For a nucleus of smaller size (Cu), one gets smaller number of partons increasing the values of $v_n^{\rm rms}$. It also slightly shifts the first peak to smaller n, due to

smaller value of $\bar{R}$. We should mention that these patterns are obtained with smaller statistics and hence are crude. One needs a more careful and detailed analysis of the effects of changing various parameters. For noncentral collisions the plot of $v_n^{\rm rms}$ (as given by the solid plot in Fig. 3) shows a peak at $n = 2$, as expected. When combined with the suppression factor of Eq. (5), it results in a double peak structure for the solid curve of Fig. 5, with similar effect for the dashed curve of Fig. 5.

We emphasize here that we are proposing a simple method for the calculation of $v_n^{\rm rms}$. These are obtained by direct calculation of variances of the distributions of v_n in the laboratory fixed frame. In the context of elliptic flow, there have been several studies on extracting elliptic flow coefficient from two-particle azimuthal correlations and how to separate the nonflow contributions [21]. Two particle azimuthal correlations, which are experimentally measured, contain contributions from nonflow effects such as jets, resonance decays, Hanbury-Brown Twiss correlations, final-state interactions, and so on. Various methods have been discussed to separate out the nonflow contributions to the azimuthal correlations [21], e.g., using cumulant expansion of multiparticle azimuthal correlations [22]. Our estimates of $v_n^{\rm rms}$ (either by direct calculation of variance, or using two particle correlations) will contain such nonflow contributions (as, for example, discussed above for the plots in Fig. 4). Though, here as one is making a plot $v_n^{\rm rms}$ for a whole range of values of n, different nonflow contributions may affect different parts of this plot. A detailed investigation of these issues is needed to separate out, or at least estimate the effects of these nonflow contributions. We hope to address these issues in a future work.

VII. CONCLUSIONS

Important aspects of our model are that we argue that important information about initial anisotropies of the system and their evolution in relativistic heavy-ion collisions can be obtained by plotting the root-mean-square values of the Fourier coefficients $v_n^{\rm rms}$ of the anisotropies in the fluctuations $\delta p/p$ of the particle momenta, calculated in a fixed laboratory frame, starting from $n = 1$ up to large values of $n \simeq 30$. Note that $n = 30$ almost corresponds to wavelength of fluctuation λ at the surface of the region, at $\tau_{\rm fr}$, being of order 1 fm. (At $\tau_{\rm eq}$ it will correspond to $\lambda \simeq 0.7$ fm.) Fluctuations with wavelengths smaller than 1 fm cannot be treated within hydrodynamical framework, so we restrict attention within this range of n. (It may be useful to plot $v_n^{\rm rms}$ for a much larger range of n. One will expect that beyond a critical value of n the nature of the curve should change in some qualitative manner indicating breakdown of underlying hydrodynamical description for smaller modes. The wavelength corresponding to that critical value of n will determine the smallest scale below which hydrodynamical description is not valid.) Important thing to note is that by taking very large number of (central) events, the root-mean-square values of v_ns can show any possible systematic variation, for example, initial rapid decrease of $v_n^{\rm rms}$ with n which eventually flattens out for large n. One needs to develop a proper understanding of this behavior (which presumably suggests a qualitative change in the nature of the fluctuations for small wavelengths) and of various factors affecting this. Further, there is the possibility of a peak near $n \sim 5$ (for Au-Au collision at 200 GeV) and of subsequent peaks for larger n. If any of these nontrivial features are detected in the particle-momentum spectra then it can open up a new way of accessing the information about initial stages of the matter produced. Just as for CMBR where the location of the first peak refers to the decoupling stage, here also the location of the first peak will give information about the freeze-out stage, including the all important equation of state that could distinguish a QGP phase from a hadronic phase. For CMBR, successive peaks yield important information about baryon content, etc., that couple to the radiation and hence contribute to the acoustic oscillations. In the same way for RHICE, if successive peaks are present, then they may give information about the detailed properties of the matter present at that stage and any dissipative factors, and so on. One important factor that can affect the shapes of these curves, especially the peaks, is the nature and presence of the quark-hadron transition. Clearly the duration of any mixed phase directly affects the freeze-out time and hence the location of the first peak. More importantly, any softening of the equation of state near the transition may affect locations of any successive peaks and their relative heights. Effects of mass ordering may also be important in this respect, especially for the behavior of these plots at large n corresponding to small λ probing very small scale fluctuations of the order of hadronic scale.

If one does see even the first peak for RHICE then one very important issue relevant for CMBR can be studied with controlled experiments. It is the issue of horizon entering. For example, by changing the nuclear size and/or collision energy, one can arrange the situation when first peak occurs at different values of n. As we have emphasized above, even the overall shape of the curve (as given by the solid plot in Fig. 3) will contain valuable information about the presence and evolution of the initial state anisotropies of the system resulting from ultrarelativistic heavy-ion collisions. It will be interesting if one can find a way to analyze the effects of such fluctuations along the longitudinal direction, i.e., with rapidity, by taking fixed azimuthal angle window. Due to rapid longitudinal expansion, presumably one will need to confine to a narrow window of rapidity. As we discussed earlier, longitudinal fluctuations are not expected to be superhorizon. Hence one may expect qualitatively different behavior in the plots of $v_n^{\rm rms}$ for this case compared to the transverse case (this is apart from the other important differences due to very different dynamics of longitudinal and transverse expansions). However, the situation may be different in the context of color glass condensate models [12]. In such models, initially a color field is established between receding nuclei, which subsequently decays in particles. If certain fluctuations are imprinted on such a color field in the longitudinal direction, then even if those are causal for the color field, for the resulting parton system, they may constitute fluctuations of superhorizon wavelengths (as the decay of the color field will involve a different time scale than the time scale of establishing the initial color field). This issue needs to be investigated in detail as it may provide a distinctive signal for color glass

condensate initial conditions. All the considerations discussed in this article can be straightforwardly applied to noncentral events, as well as for collision of nuclei that are deformed. The only difference is that for these cases certain Fourier coefficients (with small values of n) will be most dominant, as discussed above. As for the case of elliptic flow, here also it is important to estimate and measure higher moments of the flow coefficients to have a detailed understanding of the nature of the original fluctuations. Recall that these play crucial role for the CMBR analysis where non-Gaussian effects are very tightly constrained in inflationary models of density fluctuations. Similarly, in RHICE also, the physical origin of original fluctuations will constrain and determine various moments of the flow coefficients. Other issues for CMBR physics such as the effects of the thickness of the surface of last scattering on CMBR anisotropy power spectrum will have obvious implications for RHICE where also the width of the freeze-out surface will affect the plots of values of $v_n^{\rm rms}$.

ACKNOWLEDGMENTS

We are very grateful to R. Rangarajan for very useful comments and discussion. We also thank L. Sriramkumar, S. Digal, R. Ray, B. Layek, V. Tiwari, and U. Gupta for useful comments.

[1] J.-Y. Ollitrault, Phys. Rev. D **46**, 229 (1992).

[2] P. F. Kolb, P. Huovinen, U. Heinz, and H. Heiselberg, Phys. Lett. **B500**, 232 (2001); R. A. Lacey and A. Taranenko, nucl-ex/0610029; N. Borghini and J.-Y. Ollitrault, Phys. Lett. **B642**, 227 (2006).

[3] J. Adams *et al*. (STAR Collaboration), Phys. Rev. C **72**, 014904 (2005); S. S. Adler *et al*. (PHENIX Collaboration), Phys. Rev. Lett. **91**, 182301 (2003); C. Alt *et al*. (NA49 Collaboration), Phys. Rev. C **68**, 034903 (2003).

[4] M. Gyulassy, D. H. Rischke, and B. Zhang, Nucl. Phys. **A613**, 397 (1997).

[5] H. J. Drescher, F. M. Liu, S. Ostapchenko, T. Pierog, and K. Werner, Phys. Rev. C **65**, 054902 (2002); W. Broniowski, P. Bozek, and M. Rybczynski, nucl-th/0706.4266; O. Socolowski, Jr., F. Grassi, Y. Hama, and T. Kodama, Phys. Rev. Lett. **93**, 182301 (2004).

[6] B. M. Tavares, H. J. Drescher, and T. Kodama, Braz. J. Phys. **37**, 41 (2007).

[7] R. S. Bhalerao and J.-Y. Ollitrault, Phys. Lett. **B641**, 260 (2006); S. A. Voloshin, nucl-th/0606022; S. Vogel, G. Torrieri, and M. Bleicher, nucl-th/0703031; M. Miller and R. Snellings, nucl-ex/0312008.

[8] R. S. Bhalerao, J. P. Blaizot, N. Borghini, and J.-Y. Ollitrault, Phys. Lett. **B627**, 49 (2005).

[9] S. Dodelson, *Modern Cosmology* (Academic Press, San Diego, 2003).

[10] X. N. Wang and M. Gyulassy, Phys. Rev. D **44**, 3501 (1991); Comput. Phys. Comm. **83**, 307 (1994).

[11] M. Gyulassy and X. N. Wang, Nucl. Phys. **B420**, 583 (1994); X. N. Wang, M. Gyulassy, and M. Plumer, Phys. Rev. D **51**, 3436 (1995).

[12] L. McLerran, Nucl. Phys. **A787**, 1 (2007); P. Romatschke and R. Venugopalan, Phys. Rev. Lett. **96**, 062302 (2006); F. Gelis and R. Venugopalan, Nucl. Phys. **A782**, 297 (2007); Nucl. Phys. **A785**, 146 (2007).

[13] P. F. Kolb, J. Sollfrank, and U. Heinz, Phys. Rev. C **62**, 054909 (2000); P. F. Kolb and U. Heinz, *Quark Gluon Plasma 3*, edited by R. C. Hwa and X. N. Wang (World Scientific, Singapore, 2004).

[14] S. Digal and A. M. Srivastava, Phys. Rev. Lett. **80**, 1841 (1998).

[15] J.-Y. Ollitrault, Eur. J. Phys. **29**, 275 (2008).

[16] H. Petersen and M. Bleicher, Eur. Phys. J. C **49**, 91 (2007).

[17] H. J. Drescher, A. Dumitru, C. Gombeaud, and J.-Y. Ollitrault, Phys. Rev. C **76**, 024905 (2007).

[18] P. Sorensen (for the STAR Collaboration), J. Phys. G **34**, S897 (2007); S. Manly *et al*. (for PHOBOS Collaboration), nucl-ex/0702029; R. S. Hollis *et al*. (for PHOBOS Collaboration), nucl-ex/0707.0125; H. Sorge, Phys. Rev. Lett. **82**, 2048 (1999).

[19] A. K. Chaudhuri and U. W. Heinz, J. Phys. Conf. Ser. **50**, 251 (2006); R. Baier and P. Romatschke, Eur. Phys. J. C **51**, 677 (2007).

[20] P. Romatschke and U. Romatschke, Phys. Rev. Lett. **99**, 172301 (2007); D. Teaney, Phys. Rev. C **68**, 034913 (2003).

[21] N. Borghini and J.-Y. Ollitrault, Phys. Rev. C **70**, 064905 (2004); N. Borghini, P. M. Dinh, and J.-Y. Ollitrault *ibid*. **62**, 034902 (2000); P. M. Dinh, N. Borghini, and J.-Y. Ollitrault, Phys. Lett. **B477**, 51 (2000); X. Dong, S. Esumi, P. Sorensen, and Z. Xu, Phys. Lett. **B597**, 328 (2004).

[22] N. Borghini, P. M. Dinh, and J.-Y. Ollitrault, Phys. Rev. C **64**, 054901 (2001).